The 6th International Supercritical $CO_2$ Power Cycles Symposium
March 27 - 29, 2018, Pittsburgh, Pennsylvania

# Supercritical $CO_2$ Round Robin Test Program

Julie D. Tucker
Assistant Professor
Oregon State University
Corvallis, OR

Henry Saari
Associate Professor
Carlton University
Ottawa, Canada

Benjamin Adam
Graduate Research Assistant
Oregon State University
Corvallis, OR

Lucas Teeter
Graduate Research Assistant
Oregon State University
Corvallis, OR

Mark Anderson
Research Professor
University of Wisconsin
Madison, WI

Jacob Mahaffey
Postdoctoral Researcher
Sandia National Laboratories*
Albuquerque, NM, USA

Bruce Pint
Group Leader
Oak Ridge National Laboratory
Oak Ridge, TN

Ömer Doğan
Materials Research Engineer
National Energy Technology Laboratory
Albany, OR

Gordon R. Holcomb
Materials Research Engineer
National Energy Technology Laboratory
Albany, OR

Changheui Jang
Professor
Korea Advanced Institute of Science and Technology
Daejeon, South Korea

Casey S. Carney
National Energy Technology Laboratory/
AECOM
Albany, OR

Steven Kung
Technical Executive
Electric Power Research Institute
Charlotte, NC

*Sandia National Laboratories is a multimission laboratory managed and operated by National Technology and Engineering Solutions of Sandia, LLC., a wholly owned subsidiary of Honeywell International, Inc., for the U.S. Department of Energy's National Nuclear Security Administration under contract DE-NA-0003525.

**ABSTRACT**

A round robin test program has been established through DOE-NEUP to compare the corrosion results generated from several national and international supercritical carbon dioxide ($sCO_2$) test facilities. Five alloys (740H, 625, 316L, HR 120, and Grade 91) have been tested at 20 MPa and temperatures of 550°C and 700°C for times up to 1500 h. All samples are sourced from the same heats of materials and polished by a single lab to remove variability. Each organization has characterized the samples every 500 hours by weight change and oxide layer thickness. Supplemental characterization is provided by x-ray diffraction. Mass change results from the test program will be presented and discussed. Potential sources of data discrepancies will also be discussed to help shape the future of $sCO_2$ testing.

## INTRODUCTION

Growing interest in supercritical carbon dioxide ($sCO_2$) cycles is driving the need for corrosion data on candidate plant materials. The $sCO_2$ Brayton cycle (Kato2004, Oh2006) is being considered for power conversion systems including solar, fossil and nuclear heat sources. Multiple organizations have developed test facilities to address the knowledge gap in corrosion data in high temperature, high pressure $sCO_2$ environments (Firouzdor2013, Gibbs2010, Rouillard2011, Lee2014). In the past, there has been no formal test program among multiple organizations to validate the consistency of data or to make use of the different facilities to develop a consistent collaborative data generation plan. This type of testing is essential for the development of the $sCO_2$ power cycles. A demonstration of comparable and reproducible results enables a coordinated effort to explore the $sCO_2$ parameter space relevant to advanced reactor technology. This paper presents preliminary results from the round robin test plan for research grade, low flow rate $sCO_2$ corrosion testing among international organizations.

## METHODS

The $sCO_2$ testing team consists of seven organizations with $sCO_2$ corrosion testing capabilities. The organizations testing round robin samples are Oregon State University (OSU), University of Wisconsin-Madison (UW), Carleton University (CU), Korea Advanced Institute of Science and Technology (KAIST), Oak Ridge National Laboratory (ORNL), and the National Energy Technology Laboratory (NETL). The Commonwealth Scientific and Industrial Research Organization (CSIRO) is performing complementary testing on similar alloys in tube form.

The round robin team has tested five alloys with varying corrosion rates and temperature capabilities: 740H, 625, 316, HR120 and Grade 91. The chemical compositions of these alloys is provided in Table 1. Most alloys were tested at two temperatures, 550°C and 700°C. However, alloy 740H was only tested at 700°C because it is not expected to corrode significantly at 550°C. Grade 91 was only tested at 550°C because it is not considered to be suitable for 700°C applications. All samples were tested at 20 MPa in a target environment of 99.999% pure $CO_2$ (research grade). The $CO_2$ flow rates were set to refresh the test chamber at a minimum of every two hours. Each team was given six specimens of each alloy for each temperature. Samples were exposed for a total of 1500 h in 500 h increments. After each increment, all samples were removed for mass change measurements, at least one sample from each alloy was kept for additional characterization and the remainder were returned to an autoclave for additional exposure. Table 2 summaries the exposure test matrix.

Table 1. Alloy compositions (wt.%)

| Alloy | Fe | Cr | Ni | Co | Al | Mn | Mo | Nb | Cu | Ti | Si | V | W |
|---|---|---|---|---|---|---|---|---|---|---|---|---|---|
| **Gr 91** | 89.27 | 8.23 | 0.13 | 0.018 | 0.010 | 0.45 | 0.93 | 0.063 | 0.091 | 0.003 | 0.279 | 0.196 | 0.141 |
| **316L** | 68.29 | 16.84 | 9.93 | 0.214 | <0.002 | 1.58 | 1.98 | 0.009 | 0.492 | 0.010 | 0.360 | 0.079 | 0.065 |
| **HR120** | 34.48 | 24.94 | 37.44 | 0.248 | 0.069 | 0.80 | 0.47 | 0.561 | 0.065 | 0.015 | 0.483 | 0.036 | 0.078 |
| **625** | 3.66 | 21.17 | 61.65 | 0.178 | 0.204 | 0.28 | 8.70 | 3.422 | 0.159 | 0.210 | 0.168 | 0.002 | 0.111 |
| **740H** | 0.11 | 24.14 | 50.42 | 20.421 | 1.312 | 0.23 | 0.31 | 1.559 | 0.002 | 1.374 | 0.153 | 0.008 | <0.002 |

Table 2. Round robin corrosion coupon exposure matrix

| Alloy | Temperature | Exposure Time (h) |
|---|---|---|
| Grade 91 | 550°C only | 500, 1000, 1500 |
| 316L | 550°C and 700°C | 500, 1000, 1500 |
| HR 120 | 550°C and 700°C | 500, 1000, 1500 |
| 625 | 550°C and 700°C | 500, 1000, 1500 |
| 740H | 700°C only | 500, 1000, 1500 |

Prior to exposure, samples were machined from plates into 16 mm square samples with thicknesses ranging from 1.1 to 3.2 mm. A 4 mm hole was drilled in each sample for hanging in an autoclave. All samples were polished identically to a surface finish between 15-30 µm and delivered to the testing organizations. An extra sample of each alloy was prepared for as-received characterization to serve as a baseline of comparison for the exposed coupons. As-received samples were polished to 0.04 µm finish with colloidal silica, after which they were ultrasonically cleaned with methanol for 10 min.

All samples were weighed and dimensioned prior to any $sCO_2$ exposure. After each exposure increment, samples were weighed again to detect changes in mass due to corrosion product growth or spallation. A minimum of one sample was kept for further characterization after each exposure. Other samples were returned to the autoclave for additional exposure. Sample surfaces were characterized by x-ray diffraction (XRD) to assist with phase identification of corrosion products and scanning electron microscopy (SEM) were used to identify pitting or spallation of the corrosion layer. After surface characterization, samples were gold/copper coated to protect the surface and mounted in cross section to examine the thickness and chemical composition of the corrosion layer via SEM and energy dispersive spectroscopy (EDS). The mass change of each sample and the oxide thickness for one representative sample per alloy were recorded by each team after each exposure. Additional characterization by other methods; *i.e.,* transmission electron microscopy (TEM), Auger electron spectroscopy (AES), x-ray photoelectron spectroscopy (XPS), were performed as needed. Table 3 summarizes the characterization test plan.

Table 3. Round robin characterization matrix

| Characterization | As Received | 500h | 1000h | 1500h |
|---|---|---|---|---|
| **Weight** | X | x | X | x |
| **SEM-EDS** | x | x | X | x |
| **XRD** | x | As needed | As needed | As needed |
| **TEM** | As needed | As needed | As needed | As needed |
| **AES/XPS** | As needed | As needed | As needed | As needed |

## RESULTS AND DISCUSSION

*As-Received Characterization*

The as-received samples have been characterized by wide angle XRD and electron microscopy techniques for grain size analysis and microstructural assessment. The wide angle X-ray diffraction results are presented in Figure 1. It is apparent from this graph that all austenitic alloys, 740H, 625, 316L and HR 120, show peaks corresponding with austenite peak angles and ratios. However, it appears that alloy 625 has a slight deviation in location and increased intensity than the other austenitic alloys, but better aligned with the standard peaks for austenite. This is likely due to the increased Ni levels, maximizing the austenite stability and approximating the lattice parameter for pure austenite, *i.e.,* pure Ni for example. The ferritic alloy, Grade 91, shows good agreement with the standard peaks for α-ferrite, as expected for its mainly ferritic matrix.

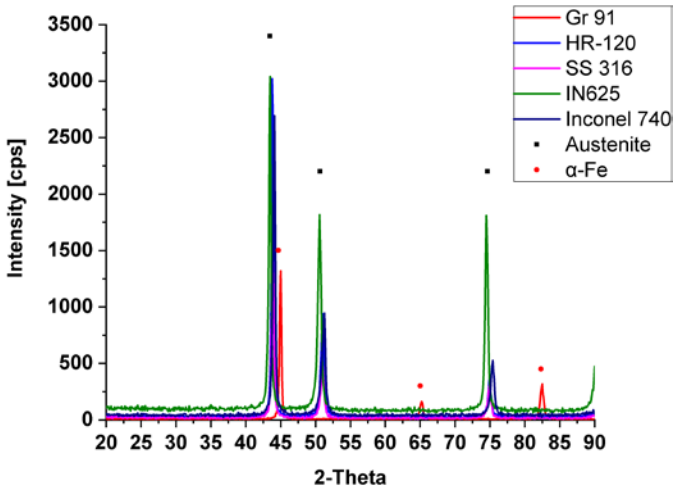


Figure 1. Wide angle X-ray spectra for all five test alloys in the as received condition, superimposed with peak markers for γ-austenite and α-ferrite, step size 0.1° and dwell time 0.1s

Since the change in microstructure of the base metal and its local chemistry are of primary concern for subsequent exposure tests, imaging of the cross sections of the as-received samples was performed to establish a reference point, seen in Figure 2. Note that, alloy Gr 91 has a much finer microstructure and was thus imaged at a higher magnification in order to adequately showcase the grain structure.

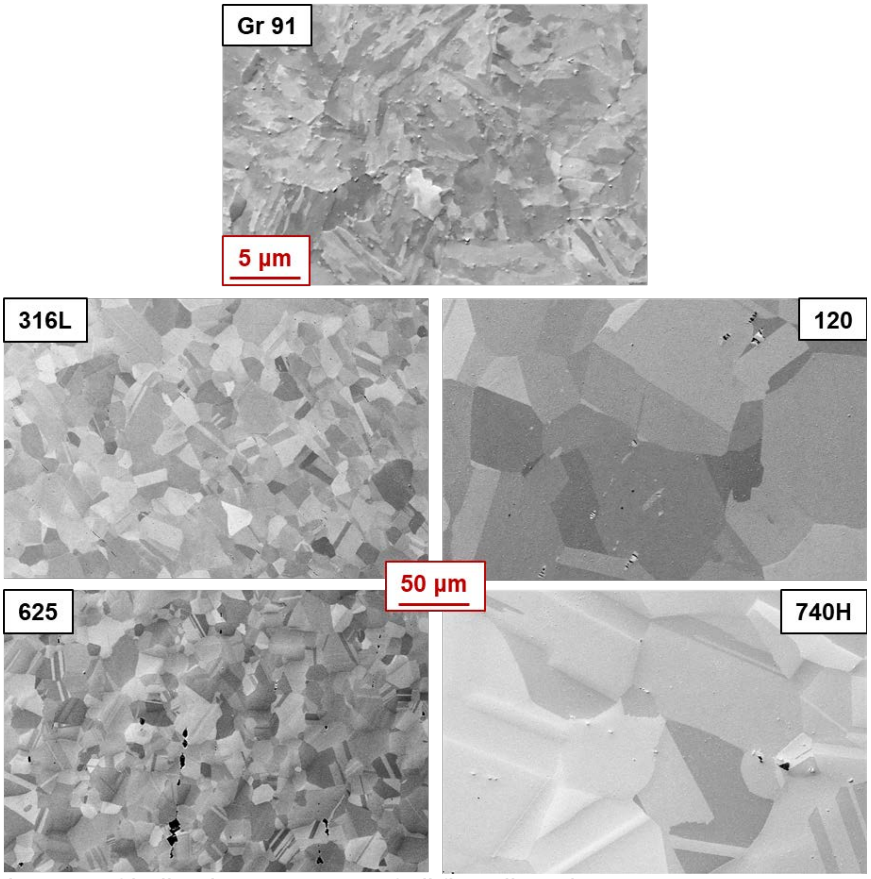


Figure 2. SEM images of bulk microstructures of all five alloys (Gr 91, 316L, HR 120, 625 and 740H) in the as-received condition

Further characterization for the as-received test alloys involved grain size analysis, for which electron back scatter diffraction (EBSD) was chosen to allow for large area scans and accurate determination of grain boundary types and registration. For convenience, all maps are displayed along the x-axis as inverse pole figure (IPF) images in Figure 3, with magnifications suitable for meaningful grain size analysis in terms of statistical number of grains in the field of view. All maps were acquired at with a Zeiss FE-SEM at an accelerating voltage of 15 kV at a 120 µm aperture and an Oxford Nordlys Nano EBSD detector. The acquisition results are shown in Table 4, with the normalized hit rate for the assumed body-centered cubic and face-centered cubic solutions. The hit rate value indicates where successful indexing was performed. Here, MAD means the mean angle deviation between fit and solution and the grain size numbers. It is worth noting that the large standard deviations for the grain areas are due to stark size difference between twins, for all alloys except Gr 91. In the case of Gr 91, the large standard deviations are due to a generally large range of grain sizes, which is also expected base on its as-received heat treatment.

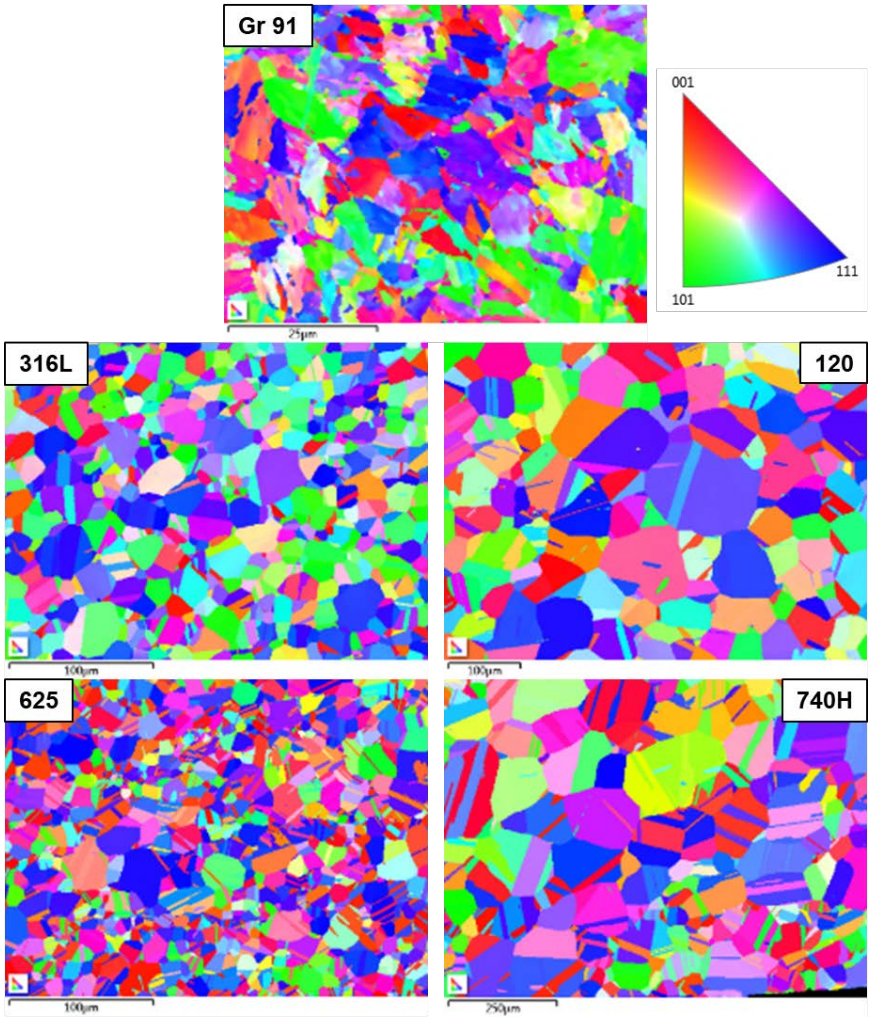

Figure 3. EBSD IPF-X maps for alloy Gr 91, 316L, HR-120, 625 and 740H

Table 4. Acquisition results for EBSD maps on bulk microstructures of all five as-received round robin test alloys, with hit rate, mean area deviation (MAD), ASTM grain size number, equivalent circle diameter (ECD) and standard deviation (SD) for grain areas and ECD

| Samples | Norm. hit rate [%] | Mean MAD | ASTM no. | Mean ECD [µm] | SD ECD [µm] | Mean area [µm$^2$] | SD area [µm$^2$] |
|---|---|---|---|---|---|---|---|
| 625 | 100 | 0.47 | 10.3 | 9.56 | 5.58 | 96.23 | 120.95 |
| 316L | 100 | 0.52 | 9.9 | 11.41 | 6.47 | 135.08 | 160.72 |
| HR-120 | 100 | 0.55 | 5.9 | 43.63 | 27.73 | 2094 | 2499 |
| 740H | 99.44 | 0.51 | 4.8 | 62.93 | 42.43 | 4516 | 5711 |
| Gr 91 | 99.88 | 0.44 | 14.8 | 1.98 | 1.3 | 4.41 | 7.47 |

*Post Exposure Characterization*

All round robin test alloys were exposed to $sCO_2$ at 550°C and/or 700°C in 500 h increments. After each exposure, the samples were weighed and compared to their original weight. Figures 4 and *5* summarize the mass change for each alloy with exposure by institution. Note that, some round robin exposure tests are still underway.

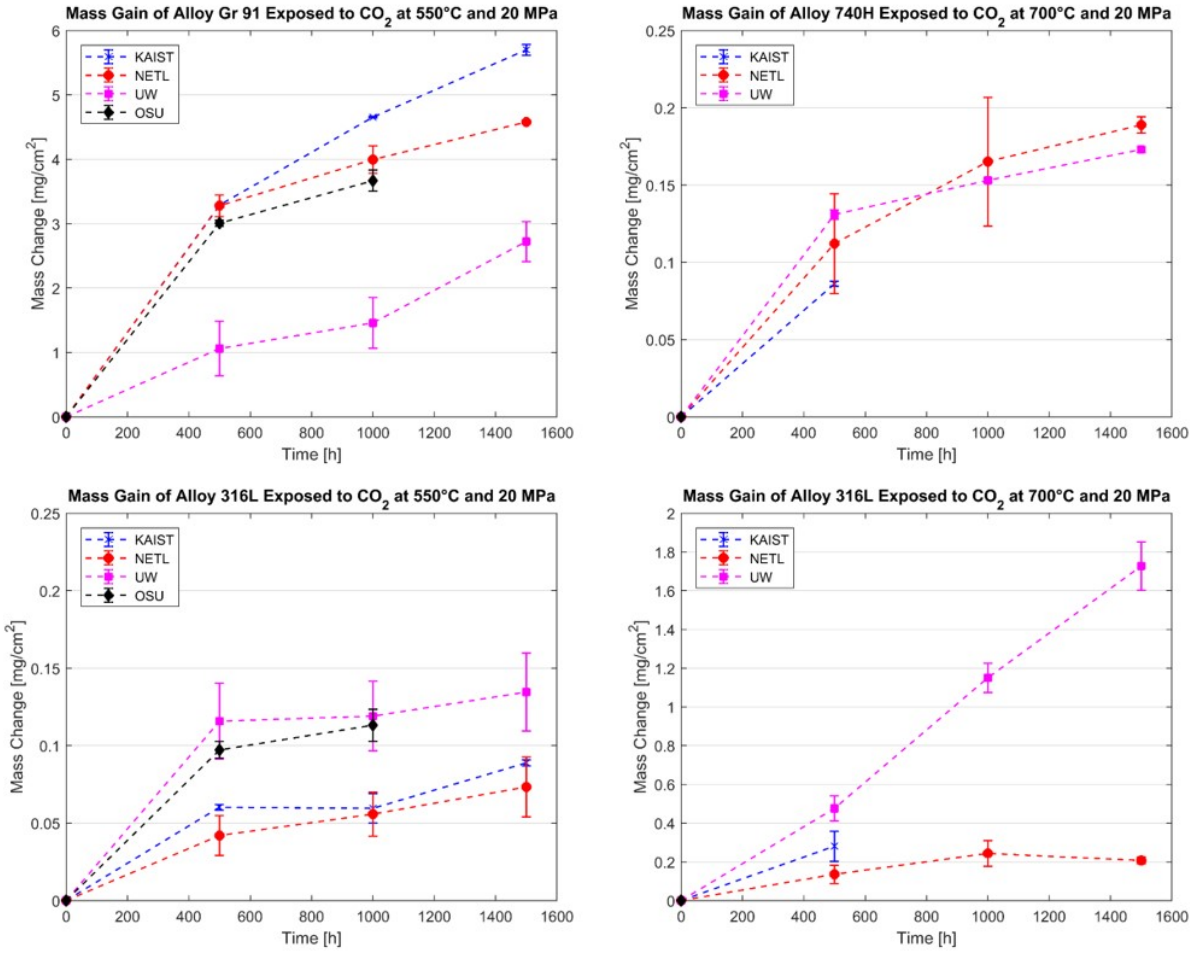


Figure 4. Mass change for all exposures to date at 550°C (left) and 700°C (right) for alloys G91, 740H and 316L

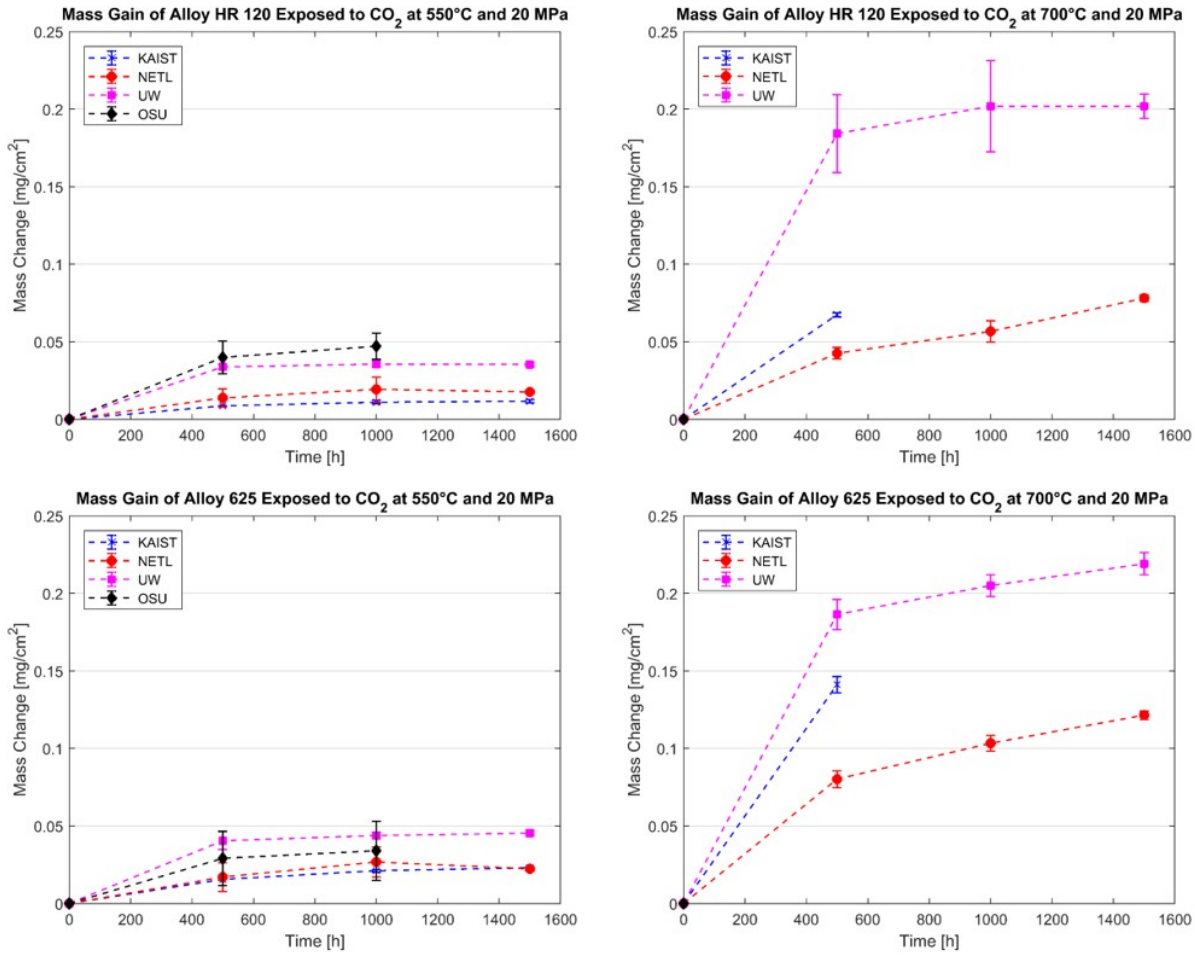


Figure 5. Mass change for all exposures to date at 550°C (left) and 700°C (right) for alloys HR120 and 625

Generally, mass change measurements across institution are in good agreement under conditions with lower amounts of mass change. As the amount of mass change increases, with higher temperatures or for less corrosion resistant alloy G91, differences between organizations are more noticeable. However, there is no consistent trend in ranking of organizations at 550°C, which suggests the differences in mass change are not systematic. At 700°C, UW is often the highest and NETL is the lowest in mass change measurements, however for alloy 740H, both institutions produce similar data. In most cases, the slope of the mass change is similar across institutions even if the absolute value is not. This indicates a similarity in corrosion rate predictions across institutions. Figures 6 and 7 replot the mass change data, assuming a parabolic growth rate. The parabolic rate constant ($K_p$) is calculated as the square of the slope of the line fit to each institution's data. Table 5 summarizes the parabolic rate constants for each institution and exposure condition from the available data.

Table 5. Parabolic rate constant $K_p$(mg$^2$/cm$^4$-s) for all conditions and institutions to date

| | 550°C | | | | 700°C | | | |
|---|---|---|---|---|---|---|---|---|
| Institution | G91 | 316L | HR 120 | 625 | 316L | HR 120 | 625 | 740H |
| KAIST | 6.3E-06 | 7.8E-10 | 9.6E-12 | 5.9E-11 | - | - | - | - |
| NETL | 1.7E-06 | 9.0E-10 | 3.0E-11 | 7.6E-11 | 1.2E-08 | 1.1E-09 | 1.8E-09 | 6.9E-09 |
| UW | 2.6E-06 | 2.9E-10 | 2.9E-12 | 2.6E-11 | 1.7E-06 | 4.0E-10 | 1.1E-09 | 1.8E-09 |
| OSU | 1.4E-06 | 8.4E-10 | 1.7E-10 | 7.9E-11 | - | - | - | - |
| Average | 3.0E-06 | 7.0E-10 | 6.1E-11 | 6.0E-11 | 8.5E-07 | 7.4E-10 | 1.4E-09 | 4.3E-09 |
| Std. Dev. | 2.2E-06 | 2.8E-10 | 9.4E-11 | 2.4E-11 | 1.2E-06 | 4.9E-10 | 4.8E-10 | 3.6E-09 |

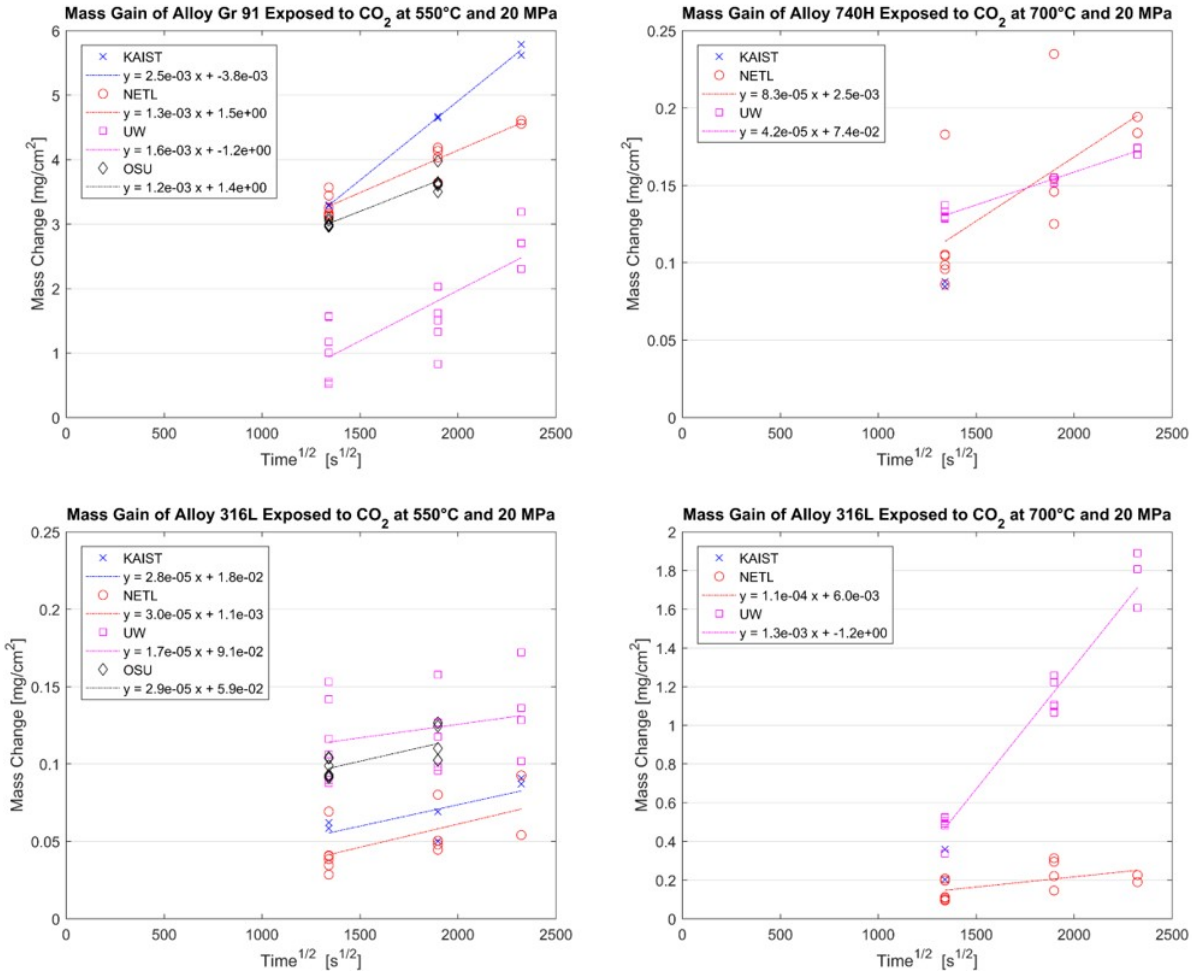


Figure 6. Parabolic rate fit at 550°C (left) and 700°C (right) for alloys G91, 740H and 316L

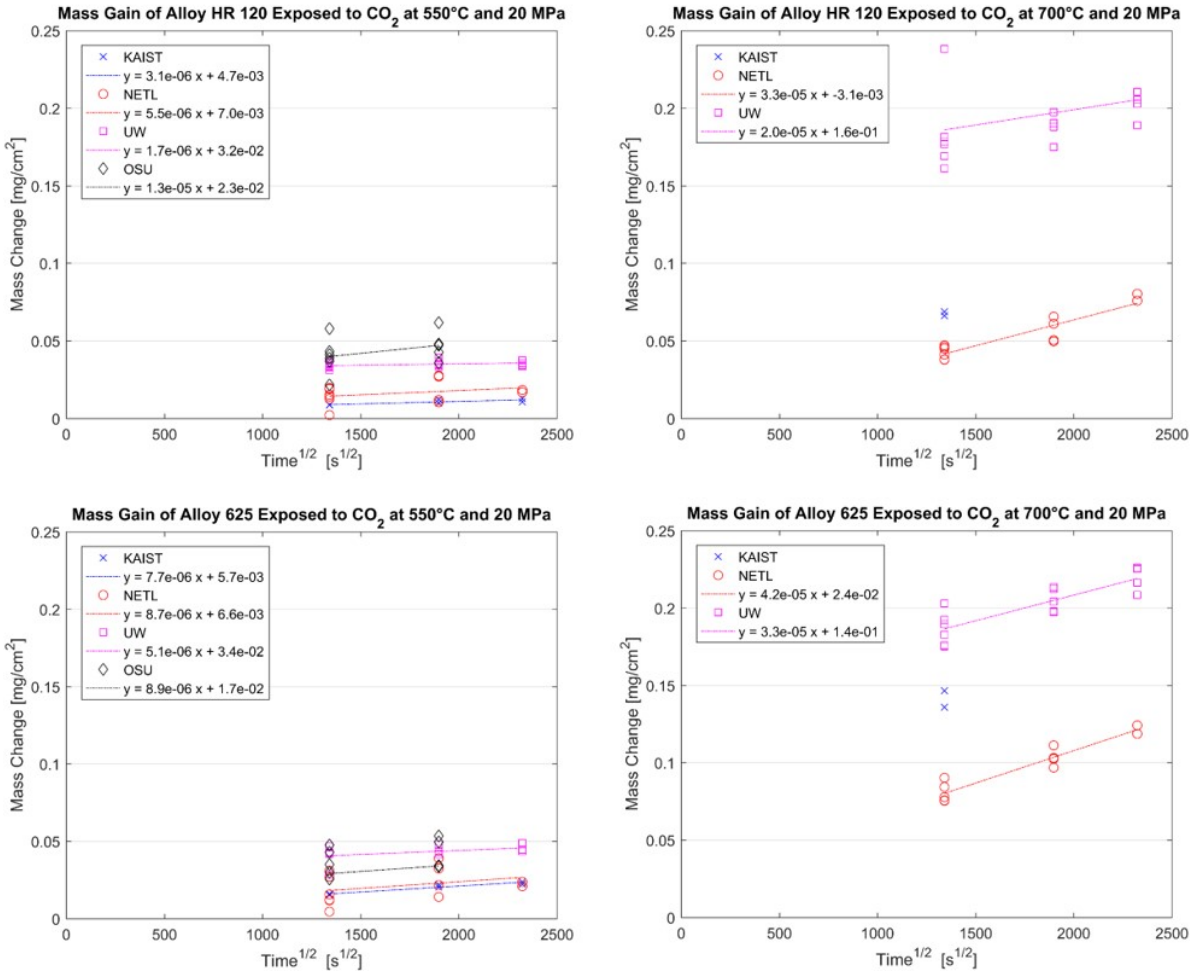

Figure 7. Parabolic rate fit at 550°C (left) and 700°C (right) for alloys HR 120 and 625

The largest differences in mass gain and parabolic rate constants are observed for alloy Gr 91 at 550°C and alloy 316L at 700°C. As expected, Gr 91 has the highest mass gain and corrosion rate of all the alloys tested, which allows for more variability between groups to be revealed. Mass changes and corrosion rates for alloy 316L at 550°C are in relatively good agreement among the institutions reporting, however, significant differences emerge at 700°C. The UW data indicates breakaway corrosion but the NETL data suggests parabolic growth. Additional data from other institutions will help to clarify the dominant behavior.

Figures 8 and 9 compares the round robin mass gain data to available literature data using the Larson-Miller parameter (P). Data is reported for exposures in both commercial grade (CG) and research grade (RG) $CO_2$. Some data presented also include impurities (IM) in the $CO_2$. Figure 8a for Gr 91, shows the round robin data is in good agreement with existing literature data, though one group of data is lower. For alloy 91, the RG or CG $CO_2$ purity does not significantly affect the mass gain, however, $O_2$ impurities in the $CO_2$ result in lower mass gains at lower values of P. At higher values of P, pure and impure $CO_2$ mass gain results start to converge. In Figure 8b for alloy 316, the round robin data is in good agreement with literature data. Trends for the role of impurities are not clear based on the available data. There does not seem to be a significant difference in mass gain caused by RG or CG $CO_2$ purity, though data is limited. Figure 8c shows the results for alloy HR 120, where the literature data is more limited. The round robin data has slightly lower mass gain than the existing data set.

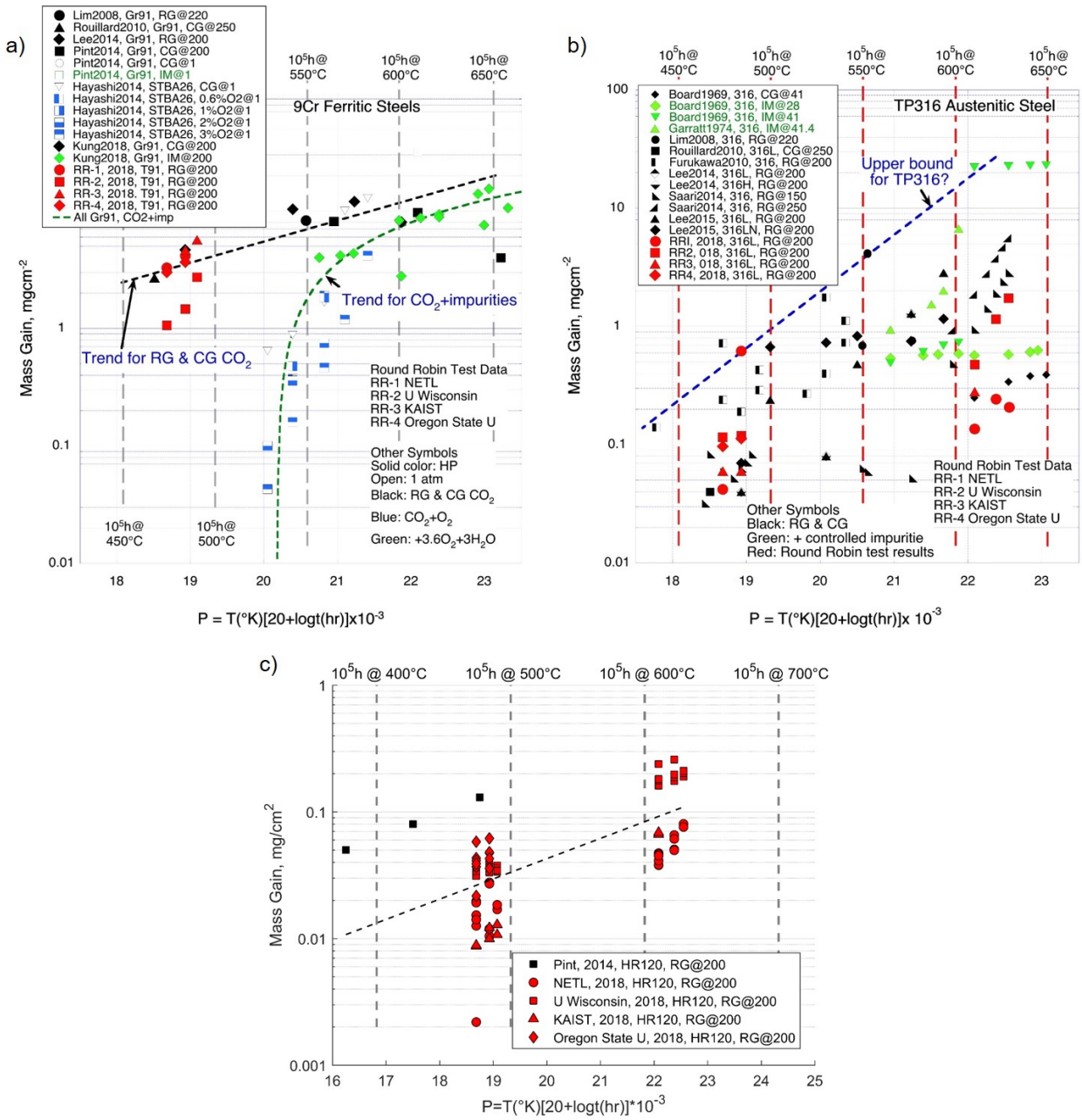


Figure 8. Round robin and literature data comparison for mass gain as a function of Larson-Miller parameter for alloy a) Gr 91 b) 316L c) HR 120

In Figure 9a, the round robin data is in good agreement with literature data for alloy 625. The CG $CO_2$ data generally has lower mass gain than the RG data. In Figure 9b, the round robin data is higher than most of the existing data but the available data on alloy 740H is limited and most data points are taken at lower pressure. There is no obvious effect of impurities on weight gain in 740H.

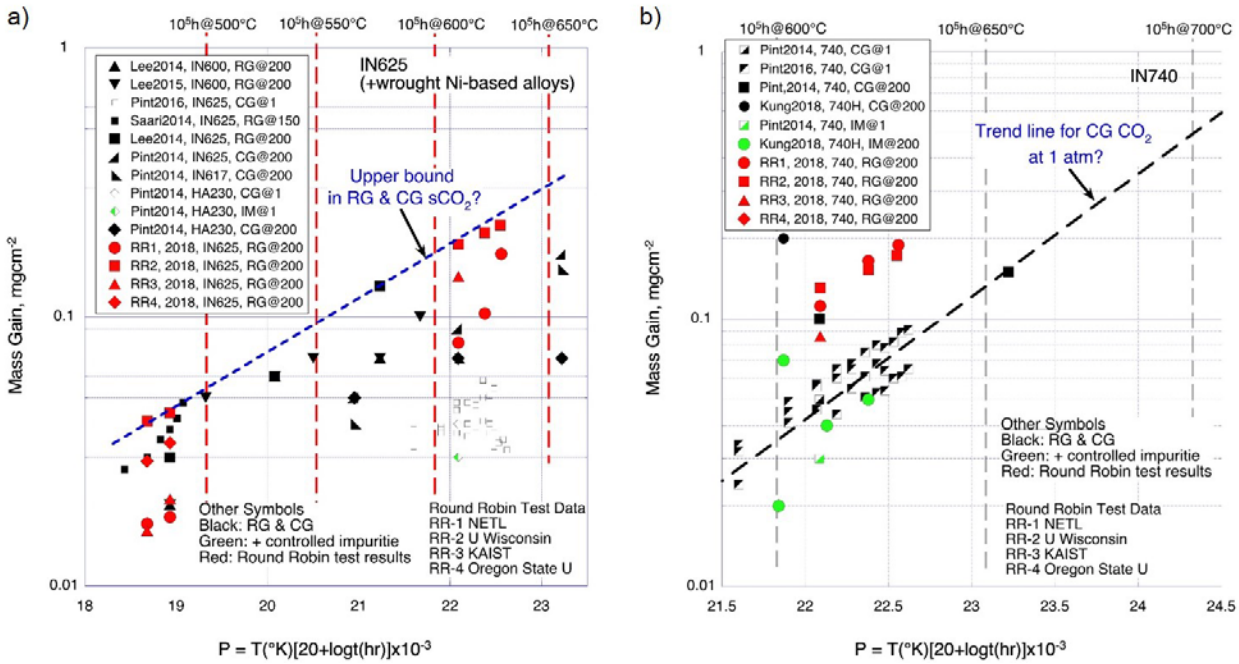


Figure 9. Round robin and literature data comparison for mass gain as a function of Larson-Miller parameter for alloy a) 625 and b) 740H

## CONCLUSION

In summary, the $sCO_2$ round robin test program has been conducted to compare corrosion results for various autoclaves around the world. Mass change data available to date has shown reasonable agreement among teams and with existing literature data. There are some discrepancies between data sets on alloys with higher corrosion rates (G91 at 550°C and 316L at 700°C). The higher mass change shown by the UW group for 316L is consistent with data generated under similar conditions (Saari2014) shown in Figure 8b. Additional data from more round robin teams and future oxide analysis will help to clarify sources of discrepancies.

## ACKNOWLEDGMENTS

The authors would like to acknowledge Ian Wright and the EPRI-DOE University Turbine Systems Research (UTSR) Project for assistance in gathering data for the Larson-Miller plots.

## REFERENCES

Kato2004: Y. Kato, T. Nitawaki, Y. Muto, Medium Temperature Carbon Dioxide Gas Turbine Reactor, Nuclear Engineering and Design 230 (2004).

Oh2006: C.H. Oh, T. Lillo, W. Windes, e. al., Development of a Supercritical Carbon-Dioxide Brayton Cycle: Improving VHTR Efficiency and Testing Materials Compatibility, Idaho National Laboratory, 2006.

Firouzdor2013: V. Firouzdor, K. Sridharan, G. Cao, M. Anderson, T.R. Allen, Corrosion of a stainless steel and nickel-based alloys in high temperature supercritical carbon dioxide environment, Corrosion Science 69 (2013) 281-291.

Gibbs2010: J.P. Gibbs, Corrosion of various engineering alloys in supercritical carbon dioxide, Massachusetts Institute of Technology, 2010.

Rouillard2011: F. Rouillard, F. Charton, G. Moine, Corrosion Behavior of Different Metallic Materials in Supercritical Carbon Dioxide at 550 degrees C and 250 bars, Corrosion 67(9) (2011).

Lee2014: H.J. Lee, C.H. Jang, Corrosion Behaviors of Structural Materialsin High Temperature S-CO2 Environments, Corrosion Science and Technology 13(2) (2014) 41-47.

Board1969: J. Board and R. Winterborne, "Oxidation of austenitic stainless steel boiler tubing in carbon dioxide," British Corrosion Journal 4 (2), 86-93 (1969).

Garrett1974: J.C.P. Garret, S.K. Lister, P.J. Nolan and J.T. Crook, "Some factors in the oxidation of austenitic stainless steels," Paper No. 23 in Proc. B.N.E.S. Intl. Conf. on Corrosion of Steels in $CO_2$ (1974).

Lim2008: J.Y. Lim, T.J. McKrell, G. Eastwick, and R.G. Ballinger, "Corrosion of materials in supercritical carbon dioxide environments," Paper no. 08430, NACE International Corrosion Conference and Expo, 2008.

Furukawa2010: T. Furukawa, Y. Inagaki, and M. Aritomi, "Corrosion behavior of FBR structural materials in high-temperature supercritical carbon dioxide," J. Power and Energy Systems, 4 (1), 252-261 (2010).

Rouillard2010: F. Rouillard, F. Charton and G. Moine "Corrosion behavior of different metallic materials in supercritical $CO_2$ at 550°C and 250 bar," Paper no. 10195, International NACE Corrosion Conference and Expo, 2010.

Hayashi2014: K. Kaya, S. Hayashi, and S. Ukai, "High-temperature oxidation behavior of Fe-9Cr steel in $CO_2$-$O_2$ gas mixture," ISIJ International, 54 (6), 1379-1385 (2014).

Lee2014: H.J. Lee, H. Kim, and C. Jang, "Compatibility of candidate structural materials in high-temperature S-$CO_2$ environment," Paper no. 32 presented at the 4th International Symposium - Supercritical $CO_2$ Power Cycles, September 9-10, 2014, Pittsburgh, Pennsylvania.

Pint2014: B.A. Pint and J.R. Keiser, "The effect of temperature on the s$CO_2$ compatibility of conventional structural alloys," Paper no. 61 presented at the 4th International Symposium - Supercritical $CO_2$ Power Cycles, September 9-10, 2014, Pittsburgh, Pennsylvania.

Saari2014: H. Saari, C. Parks, R. Petruskeno, B. Maybee, and K. Zanganeh, "Corrosion testing of high-temperature materials in supercritical $CO_2$," Paper no. 32 presented at the 4th International Symposium - Supercritical $CO_2$ Power Cycles, September 9-10, 2014, Pittsburgh, Pennsylvania.

Lee2015: H.J. Lee, H. Kim, S.H. Kim, and C. Jang, "Comparison of the corrosion behaviors of Fe-base and Ni-base austenitic alloys in high-temperature S-$CO_2$ environment," Section 3, Session 1A-Supercritical $CO_2$ Oxidation/Corrosion, Proc. EPRI International Conference on Corrosion in Power Plants (San Diego, Oct 13-15, 2015), EPRI Report No. 3002006972, Nov. 2015.

Pint2016: B.A. Pint, "ORNL SunShot Concentrated Solar Power Supercritical $CO_2$ Lifetime Model Project Overview," presentation to Concentrated Solar Power Industry Group, Apr 13, 2016.

Kung2018: S.C. Kung, J.P. Shingledecker, B.M. Tossey, I.G. Wright, T. Lolla, and A.S. Sabau, "Corrosion of heat exchanger alloys in open-fired s$CO_2$ power cycles," 6th International Supercritical $CO_2$ Power Cycles Symposium, March 27 - 29, 2018, Pittsburgh, Pennsylvania.